Analytical solution of the heat equation in a longitudinally pumped cubic solid-state laser

Mohammad Sabaeian,[1] Hamid Nadgaran,[1,*] and Laleh Mousave[2]

[1]Physics Department, College of Science, Shiraz University, Shiraz 71454, Iran

[2]Physics Department, Azad University of Dezful, Dezful, 313, Iran

*Corresponding author: nadgaran@susc.ac.ir

Received 11 February 2008; accepted 26 March 2008;
posted 2 April 2008 (Doc. ID 92652); published 28 April 2008

Knowledge about the temperature distribution inside solid-state laser crystals is essential for calculation of thermal phase shift, thermal lensing, thermally induced birefringence, and heat-induced crystal bending. Solutions for the temperature distribution for the case of steady-state heat loading have appeared in the literature only for simple cylindrical crystal shapes and are usually based on numerical techniques. For the first time, to our knowledge, a full analytical solution of the heat equation for an anisotropic cubic cross-section solid-state crystal is presented. The crystal is assumed to be longitudinally pumped by a Gaussian pump profile. The pump power attenuation along the crystal and the real cooling mechanisms, such as convection, are considered in detail. A comparison between our analytical solutions and its numerical counterparts shows excellent agreement when just a few terms are employed in the series solutions. © 2008 © 2008 Optical Society of America

OCIS codes: 120.6780, 120.6810, 140.3580, 140.3480.

1. Introduction

Thermal effects in solid-state lasers are unavoidable, particularly when the laser medium is pumped by high-power beams. Nonradiative relaxations and quantum defects are mainly responsible for thermal effects [1]. Mechanisms such as concentration quenching [2] and energy transfer upconversion [3] are also named as other heating contributors. The induced heat load of the lasing medium needs much attention when the pump beam is focused to a small size. The requirement for a tightly focused beam leads to a high pump deposition energy and a high thermal loading density. The laser crystal then suffers various thermomechanical and thermo-optical effects such as thermal lensing, birefringence, and heat-induced crystal bending [4–6]. In this regard, there are many publications that are especially devoted to thermal effects in laser crystals. Among them, Sabaeian and Nadgaran [7] have demonstrated not only that these thermal effects play crucial roles in generating laser beams, but also that they are even much stronger and more influential in generating other laser beam families such as Bessel–Gauss beams. Thus modeling of thermal problems is seen to be an important issue that addresses the thermally induced effects. The value of such models is heavily dependent on the temperature distribution function for the laser crystal and the more realistic boundary conditions used. Most attempts so far for modeling these effects, however, are based on the temperature distribution obtained for just simple cylindrical crystal shapes [6,8–10], and research studies had to use these cylindrical-based solutions even for cubic cross-section crystals [11–13]. Only recently, the thermal effects of a Nd : YVO_4 slab laser was reported by Ma *et al.* [14]. Although they pointed out many important parameters influencing the thermal model, their model is based on simple boundary conditions in which

0003-6935/08/132317-09$15.00/0

the slab was assumed to be infinitely long along one of the axes of the Cartesian coordinate system. Shi *et al.* [15] also reported the solution of the heat equation for a cubic geometry. They, too, adopted a simple boundary condition in which the temperature of all six faces was taken to be zero and constant. Although they solved the heat equation skillfully by including the pump attenuation term, the assumption of constant temperature for all faces, particularly for end faces, should be reconsidered.

The main aim in the present paper is to present a comprehensive analytical solution of the heat equation for an anisotropic crystal of cubic geometry, since the temperature distribution function is essential in calculation, simulation, and prediction of thermal effects. Through comprehensive comparison of the analytical solutions with the numerical one, one can confirm that this analytical solution possesses a considerable level of reliability that can be elegantly employed in complicated thermal analysis of laser media. Here longitudinal diode pumping is assumed because of the many advantages that this technique has over other pumping techniques. Among these advantages, one can name the availability of high lasing efficiencies, enormous flexibility in the resonator design, diversity of the operating wavelengths, and relative ease with which fundamental transverse mode and linearly polarized operation can be selected [1]. Our results were specifically applied to Nd : YVO_4 crystal, which has proved to be a promising laser medium [13–18] because of its large stimulating emission cross section at the 1064 nm wavelength, broad absorption band at 808 nm, strong pump absorption [19], and good thermal conductivity [11]. The crystal was assumed to be pumped by a Gaussian pump profile, and realistic mechanisms of cooling of end faces and lateral faces of the cube were considered in detail. In this respect, three different cases were adopted for obtaining a complete solution to the heat equation. First, a case in which the four lateral faces were kept at a constant temperature equal to the ambient temperature was investigated. In this case convection was allowed to cool the end faces. In the second case, a constant temperature different from the ambient temperature was assumed for the four lateral faces, and convection still cools the end faces. Obviously, the above two cases are related to a so-called perfect cooling mechanism. Finally, we have solved the heat equation for a general case in which a convection cooling mechanism for all six faces was assumed. In this generalized case we took different heat transfer coefficients for the lateral and end faces. The results were applied to a Nd : YVO_4 crystal and were compared with the results of the numerical solutions. The comparison not only shows very good agreement between the two methods but also indicates considerable reliability of the analytical expressions.

2. Heat Equation

The general steady-state heat equation for an anisotropic cubic solid in Cartesian coordinates is given by [19]

$$K_x \frac{\partial^2 T(x,y,z)}{\partial x^2} + K_y \frac{\partial^2 T(x,y,z)}{\partial y^2} + K_z \frac{\partial^2 T(x,y,z)}{\partial z^2} = -S(x,y,z), \tag{1}$$

where T is temperature, K_x, K_y, and K_z are three different thermal conductivities along x, y, and z axes, respectively, and S is the heat source density in watts per meter. In the case of end pumping, the source term for a crystal with dimensions $a \times b \times c$ can be written as [5]

$$S(x,y,z) = Q_0 \exp\left\{-2\left[\left(x-\frac{a}{2}\right)^2 + \left(y-\frac{b}{2}\right)^2\right]/\omega_p^2\right\} \exp(-\gamma z) \tag{2}$$

with

$$Q_0 = \frac{2\eta P}{\pi\omega_p^2(1-e^{-\gamma c})\operatorname{erf}\left(\frac{a\sqrt{2}}{2\omega_p}\right)\operatorname{erf}\left(\frac{b\sqrt{2}}{2\omega_p}\right)}, \tag{3}$$

where ω_p is the pump beam spot size and γ is the pump beam absorption coefficient. In Eq. (3) $\eta = 1 - \lambda_p/\lambda_l$ is the quantum defect, in which λ_p (λ_l) is the pump (laser) wavelength. Also, P stands for absorbed pump power and $\operatorname{erf}(x)$ for the error function defined by $\operatorname{erf}(x) = 2/\sqrt{\pi}\int_0^x e^{-t^2}\,dt$ [20].

3. Boundary Conditions and Solutions

Figure 1 shows our three-dimensional crystal cube. As in all three cases mentioned above, the two end faces of the crystal are cooled by convection; the following boundary conditions were assumed [21]:

$$K_z \frac{\partial T(x,y,z)}{\partial z}\bigg|_{z=0} = h_a[T(x,y,z=0) - T_0] \tag{4}$$

for the $z = 0$ end face and

$$-K_z \frac{\partial T(x,y,z)}{\partial z}\bigg|_{z=c} = h_a[T(x,y,z=c) - T_0] \tag{5}$$

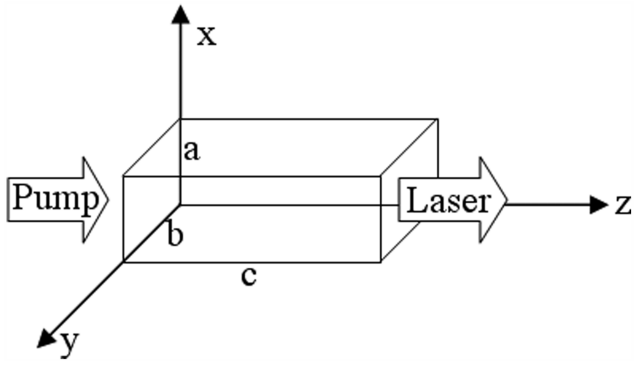

Fig. 1. Schematic of cubic geometry crystal.

for the $z = c$ end face. Here, h_a is the heat transfer coefficient for end faces and T_0 is the ambient temperature.

Depending on the cooling system, the boundary conditions would be different for the four lateral faces. They may be kept at a constant temperature or be cooled by convection. These cases will be investigated in the next subsections.

A. Case I: Same Constant Temperature for the Four Lateral Faces

In this case, it is assumed that the four lateral faces of the cube are kept in thermal equilibrium with the ambient, so the proper boundary conditions can be written as [15]

$$T(x=0,y,z) - T_0 = T(x=a,y,z) - T_0 = 0, \tag{6}$$

$$T(x,y=0,z) - T_0 = T(x,y=b,z) - T_0 = 0. \tag{7}$$

Equations (6) and (7) together with Eqs. (4) and (5) form a complete set of boundary conditions for this case. The temperature distribution in the crystal that satisfies the above boundary conditions can be expressed as

$$T(x,y,z) = \sum_{m,n=1}^{\infty} T_{mn}(z) \sin\left(\frac{m\pi x}{a}\right) \sin\left(\frac{n\pi y}{b}\right) + T_0, \tag{8}$$

where $T_{mn}(z)$ is a function to be found to satisfy the end faces conditions, Eqs. (4) and (5). By substituting Eq. (8) into Eq. (1), multiplying both sides by $\sin(m'\pi x/a)\sin(n'\pi y/b)$, and integrating over x and y from $x = 0 \to a$ and $y = 0 \to b$, we get

$$\frac{\mathrm{d}^2 T_{mn}(z)}{\mathrm{d}z^2} - \Gamma_{mn}^2 T_{mn}(z) = -\frac{4Q_0}{abK_z} p_m q_n e^{-\gamma z}, \tag{9}$$

where

$$\Gamma_{mn}^2 = \frac{K_x}{K_z}\left(\frac{m\pi}{a}\right)^2 + \frac{K_y}{K_z}\left(\frac{n\pi}{b}\right)^2, \tag{10}$$

$$\begin{aligned} p_m &= \int_0^a e^{-2(x-a/2)^2/\omega_p^2} \sin(m\pi x/a)\mathrm{d}x \\ &= \frac{\sqrt{2\pi}\omega_p}{2} e^{-m^2\pi^2\omega_p^2/8a^2} \sin\left(\frac{m\pi}{2}\right) \\ &\quad \times \mathrm{Re}\left\{\mathrm{erf}\left(\frac{\sqrt{2}a}{2\omega_p} + i\frac{\sqrt{2}m\pi\omega_p}{4a}\right)\right\}, \end{aligned} \tag{11}$$

$$\begin{aligned} q_n &= \int_0^b e^{-2(y-b/2)^2/\omega_p^2} \sin(n\pi y/b)\,\mathrm{d}y \\ &= \frac{\sqrt{2\pi}\omega_p}{2} e^{-n^2\pi^2\omega_p^2/8b^2} \sin\left(\frac{n\pi}{2}\right) \\ &\quad \times \mathrm{Re}\left\{\mathrm{erf}\left(\frac{\sqrt{2}b}{2\omega_p} + i\frac{\sqrt{2}n\pi\omega_p}{4b}\right)\right\}. \end{aligned} \tag{12}$$

It is clear that for even values of m and n the integrals of Eqs. (11) and (12) would be zero. This decreases the number of terms in Eq. (8) by half. Equation (9) is an ordinary differential equation that can be solved by finding a general solution for its homogenous form plus a particular solution for its inhomogeneous form. The overall solution to Eq. (9) is then

$$T_{mn}(z) = A_{mn}^{+} e^{\Gamma_{mn} z} + A_{mn}^{-} e^{-\Gamma_{mn} z} - B_{mn} e^{-\gamma z}, \tag{13}$$

where the unknown coefficients A_{mn}^{+} and A_{mn}^{-} are to be found and B_{mn} coefficients are defined as

$$B_{mn} = \frac{4Q_0 p_m q_n}{abK_z(\gamma^2 - \Gamma_{mn}^2)}. \tag{14}$$

By substituting Eq. (8) into Eqs. (4) and (5), we get the following two equations:

$$K_z \left.\frac{\mathrm{d}T_{mn}}{\mathrm{d}z}\right|_{z=0} - h_a T_{mn}(z=0) = 0, \tag{15}$$

$$K_z \left.\frac{\mathrm{d}T_{mn}}{\mathrm{d}z}\right|_{z=c} + h_a T_{mn}(z=c) = 0. \tag{16}$$

Now, inserting Eq. (13) into Eqs. (15) and (16) gives us the values of A_{mn}^{+} and A_{mn}^{-} (see Appendix A).

To this end, we ended up with a compact solution of Eq. (1) for the first case, that is, Eq. (8) with all known functions.

B. Case II: Same Constant Temperature for the Four Lateral Faces, Different from the Ambient Temperature

Here, in this case, the four lateral faces are kept at T_1, different from the ambient temperature T_0. So the boundary conditions will take the form

$$T(x=0,y,z) - T_1 = T(x=a,y,z) - T_1 = 0, \tag{17}$$

$$T(x,y=0,z) - T_1 = T(x,y=b,z) - T_1 = 0, \tag{18}$$

where T_1 is the coolant temperature. Equations (17) and (18) together with Eqs. (4) and (5) form another complete set of boundary conditions suitable for this case. The initial temperature distribution takes the form

$$T(x,y,z)=\sum_{m,n=1}^{\infty}T_{mn}(z)\sin\left(\frac{m\pi x}{a}\right)\sin\left(\frac{n\pi y}{b}\right)+T_1. \tag{19}$$

In this case some of the calculation steps are similar to case I, but we end up with Eqs. (22) and (23) instead (see below).

By substituting Eq. (19) into Eqs. (4) and (5), we have

$$\sum_{m,n=1}^{\infty}\left\{\sin\left(\frac{m\pi x}{a}\right)\sin\left(\frac{n\pi y}{b}\right)\times\left(K_z\frac{\mathrm{d}T_{mn}}{\mathrm{d}z}-h_aT_{mn}\right)\Big|_{z=0}\right\}=h_a\Delta T, \tag{20}$$

$$\sum_{m,n=1}^{\infty}\left\{\sin\left(\frac{m\pi x}{a}\right)\sin\left(\frac{n\pi y}{b}\right)\left(-K\frac{\mathrm{d}T_{mn}}{\mathrm{d}z}-hT_{mn}\right)\Big|_{z=c}\right\}=h_a\Delta T, \tag{21}$$

where $\Delta T=T_1-T_0$. By multiplying both sides of Eqs. (20) and (21) by $\sin(m'\pi x/a)\sin(n'\pi y/b)$ and integrating over x and y from $x=0\rightarrow a$ and $y=0\rightarrow b$, we obtain

$$K_z\frac{\mathrm{d}T_{mn}}{\mathrm{d}z}\Big|_{z=0}-h_aT_{mn}(z=0)=\begin{cases}\frac{16h_a}{mn\pi^2}\Delta T & n,m=\text{odd}\\ 0 & \text{others}\end{cases}, \tag{22}$$

$$K_z\frac{\mathrm{d}T_{mn}}{\mathrm{d}z}\Big|_{z=c}+h_aT_{mn}(z=c)=\begin{cases}\frac{-16h_a}{mn\pi^2}\Delta T & n,m=\text{odd}\\ 0 & \text{others}\end{cases}. \tag{23}$$

Here again odd values of m and n are concerned [see Eqs. (11) and (12))]. The solutions of Eqs. (22) and (23) can provide the values of A_{mn}^{+} and A_{mn}^{-} for this case [see Appendix A, Eq. (A2)].

Despite the apparent resemblance between cases I and II, one can realize how the simple Eqs. (15) and (16) of case I are replaced by Eqs. (22) and (23) of case II. So, it is worth differentiating between the two different cases.

C. Case III: Convection for All Six Faces

Case III is the most realistic and general case in which the crystal cools via the air convection mechanism or by being in contact with an imperfect cooling system. In this case the boundary conditions take the forms [21]

$$K_x\frac{\partial T}{\partial x}\Big|_{x=0}=h_s[T(x,y,z)-T_0]_{x=0}, \tag{24}$$

$$-K_x\frac{\partial T}{\partial x}\Big|_{x=a}=h_s[T(x,y,z)-T_0]_{x=a}, \tag{25}$$

$$K_y\frac{\partial T}{\partial y}\Big|_{y=0}=h_s[T(x,y,z)-T_0]_{y=0}, \tag{26}$$

$$-K_y\frac{\partial T}{\partial y}\Big|_{y=b}=h_s[T(x,y,z)-T_0]_{y=b}, \tag{27}$$

$$K_z\frac{\partial T}{\partial z}\Big|_{z=0}=h_a[T(x,y,z)-T_0]_{z=0}, \tag{28}$$

$$-K_z\frac{\partial T}{\partial z}\Big|_{z=c}=h_a[T(x,y,z)-T_0]_{z=c}. \tag{29}$$

In the above expressions we have used two different heat transfer coefficients for lateral and end faces. We chose the initial temperature distribution expression as follows:

$$T(x,y,z)=\sum_{m,n=1}^{\infty}T_{mn}(z)\sin\left(\frac{\alpha_m x}{a}+\beta_m\right)\times\sin\left(\frac{\delta_n y}{b}+\theta_n\right)+T_0, \tag{30}$$

where α_m, β_m, δ_n, and θ_n are constants to be found to satisfy the boundary conditions of Eqs. (24)–(29).

To get the values of α_m and β_m, we first substitute Eq. (30) into Eqs. (24) and (25) and then use the linear independency properties of sinusoidal functions. We end up with

$$\tan(\beta_m)=\frac{K_x\alpha_m}{h_sa}, \tag{31}$$

$$\tan(\alpha_m+\beta_m)=-\frac{K_x\alpha_m}{h_sa}. \tag{32}$$

This is a set of nonlinear equations. If we eliminate β_m between Eqs. (31) and (32), we get

$$2\cot(\alpha_m)=\frac{K_x\alpha_m}{h_sa}-\frac{h_sa}{K_x\alpha_m}. \tag{33}$$

Equation (33) needs to be solved numerically. Then the values of β_m are

$$\beta_m = \tan^{-1}\left(\frac{K_x \alpha_m}{h_s a}\right). \tag{34}$$

In order to calculate δ_n and θ_n, we use Eqs. (26) and (27) to find a set of equations similar to Eqs. (31) and (32), as

$$\tan(\delta_n) = \frac{K_y \delta_n}{h_s b}, \tag{35}$$

$$\tan(\delta_n + \theta_n) = -\frac{K_y \delta_n}{h_s b}. \tag{36}$$

Following the approach used for finding α_m and β_m, we can find δ_n and θ_n.

To find $T_{mn}(z)$ in this case, we substitute Eq. (30) into Eq. (1), leading to

$$\frac{\mathrm{d}^2 T_{mn}(z)}{\mathrm{d}^2 z} - \Gamma_{mn}^2 T_{mn}(z) = -\frac{16 Q_0}{K_z ab} s_m t_n e^{-\gamma z}, \tag{37}$$

where

$$\Gamma_{mn}^2 = \frac{K_x}{K_z}\left(\frac{\alpha_m}{a}\right)^2 + \frac{K_y}{K_z}\left(\frac{\delta_n}{b}\right)^2, \tag{38}$$

To obtain A_{mn}^{+} and A_{mn}^{-} coefficients, we follow the approach given in Subsection 3.A. A similar treatment gives us the coefficients indicated by Eq. (A3) (See Appendix A).

In deriving Eq. (37), one may debate the orthogonal properties of sine functions appearing in Eq. (30). The proof that these sine functions are indeed orthogonal is given in Appendix B.

4. Results and Comparison with Numerical Solution

In this section, the expressions obtained in the previous sections will be applied to Nd : YVO_4 cubic crystal, and the results will be compared with their numerical counterparts obtained by finite element methods. This comparison can eventually yield the number of terms needed in Eq. (8) for a given degree of accuracy. The crystal considered was a 3 mm × 3 mm × 5 mm Nd : YVO_4 crystal block [15,19] with thermal conductivity of $K_x = K_y = 5.1\,\mathrm{W\,K^{-1}\,m^{-1}}$ and $K_z = 5.23\,\mathrm{W\,K^{-1}\,m^{-1}}$ [21]. The heat transfer coefficient of end faces was taken as $h_a = 6.5\,\mathrm{WK^{-1}m^{-2}}$. The crystal was assumed to be pumped by a Gaussian beam of $\omega_0 = 0.4\,\mathrm{mm}$ at $\lambda_p = 808\,\mathrm{nm}$ delivering a laser beam of $\lambda_l = 1064\,\mathrm{nm}$. The pump absorption coefficient at $\lambda_p = 808\,\mathrm{nm}$ is about $\gamma = 14.8\,\mathrm{cm^{-1}}$, and the absorbed pump power was taken to be $P = 15\,\mathrm{W}$.

Figure 2 shows a three-dimensional temperature distribution in the X–Y plane at $Z = 0$ under boundary conditions mentioned in Section 3. The ambient temperature is $T_0 = 300\,\mathrm{K}$, and the m and n indices

$$s_m = \frac{\int_0^a \exp[-2(x-a/2)^2/\omega_p^2)]\sin[(\alpha_m x/a)+\beta_m]\mathrm{d}x}{2-[\sin(2\alpha_m+2\beta_m)-\sin(2\beta_m)]/\alpha_m} = \frac{\sqrt{\pi/2}\,\omega_p e^{-\alpha_m^2\omega_p^2/8a^2}\sin(\beta_m+\alpha_m/2)\,\mathrm{Re}\left[\mathrm{erf}\left(\frac{\sqrt{2}a}{2\omega_p}+i\frac{\sqrt{2}\alpha_m\omega_p}{4a}\right)\right]}{2-[\sin(2\alpha_m+2\beta_m)-\sin(2\beta_m)]/\alpha_m}, \tag{39}$$

$$t_n = \frac{\int_0^a \exp[-2(y-b/2)^2/\omega_p^2)]\sin[(\delta_n y/b)+\theta_n]\mathrm{d}y}{2-[\sin(2\delta_n+2\theta_n)-\sin(2\theta_n)]/\delta_n} = \frac{\sqrt{\pi/2}\,\omega_p e^{-\delta_n^2\omega_p^2/8b^2}\sin(\theta_n+\delta_n/2)\,\mathrm{Re}\left[\mathrm{erf}\left(\frac{\sqrt{2}b}{2\omega_p}+i\frac{\sqrt{2}\delta_n\omega_p}{4b}\right)\right]}{2-[\sin(2\delta_n+2\theta_n)-\sin(2\theta_n)]/\delta_n}. \tag{40}$$

Equation (37) is similar to Eq. (9) with some differences. Its solution can be written simply as

$$T_{mn}(z) = A_{mn}^{+} e^{\Gamma_{mn} z} + A_{mn}^{-} e^{-\Gamma_{mn} z} - B_{mn} e^{-\gamma z}, \tag{41}$$

where

$$B_{mn} = \frac{16\,Q_0\,s_m\,t_n}{ab\,K_z(\gamma^2 - \Gamma_{mn}^2)}. \tag{42}$$

are $m, n = 1, 3, 5, 7, 9$, since the even values of m and n would lead to $p_m = q_n = B_{mn} = A_{mn}^{\pm} = 0$ [see Eqs. (11)–(14)].

Figure 3 shows the crystal temperature at $Z = 0$ and $Z = c/2$ ($c = 5\,\mathrm{mm}$) at $Y = b/2$ planes along the X axis. In plotting Fig. 3 we have adopted five successive odd terms in our series solution, i.e., Eq. (8). In this figure the solid curves show the results of our analytical solution, and the overlapping dotted curves show our numerical solution. As is clear from Fig. 3, there is only a tiny difference be-

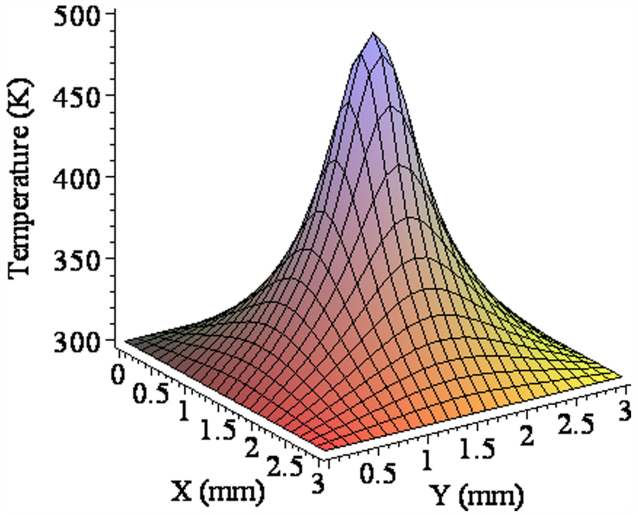

Fig. 2. (Color online) Three-dimensional temperature distribution computed by Eq. (8) in the X–Y plane at $Z = 0$ with $m, n = 1, 3, 5, 7, 9$.

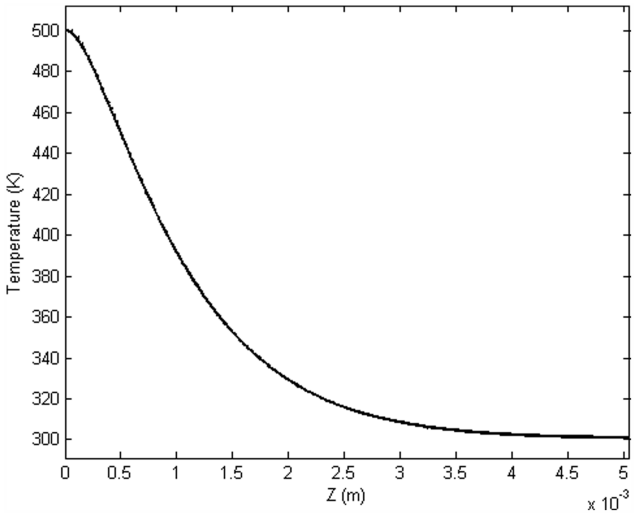

Fig. 4. Temperature distribution along the crystal axis at $X = a/2$ and $Y = b/2$. The solid curve shows the analytical solution with $m, n = 1, 3, 5, 7, 9$; the dotted curve shows the numerical calculation.

tween the analytical and numerical solution for the $Z = 0$ plane, whereas there is almost no difference between the two solutions for $Z = c/2$. Therefore, we can conclude that the analytical solution carries a very considerable reliability level when just five successive odd terms of Eq. (8) are employed. Figure 4 shows the temperature distribution along the crystal axis (Z axis) at $X = a/2$ ($a = 3\,\text{mm}$) and $Y = b/2$ ($b = 3\,\text{mm}$) for a 15 W pump power. In this figure, too, we can hardly see any difference between the analytical and numerical solutions.

Figure 5 depicts the temperature distribution along the X axis in the planes $Z = 0$ and $Z = c/2$ at $Y = b/2$ computed by Eq. (19) of case II in which the four lateral faces of the cube were kept at T_1 (= 350 K), different from the ambient temperature of T_0 (= 300 K). Here, again, five successive odd terms were included in the sum. The excellent agreement between the two calculations is apparent from the Fig. 5. Here the end faces are cooled by convection.

Figure 6 shows the three-dimensional temperature distribution calculated by Eq. (30), in which we have assumed an imperfect cooling system. For this, the lateral faces are usually wrapped by a copper shield with a cold liquid flowing around. Thus the heat transfer coefficient can vary depending on the system design. For our calculation, $h_s = 1.5 \times 10^4\,\text{W K}^{-1}\,\text{m}^{-2}$ [21], which is appropriate for a system in contact with copper. In Fig. 6, the curves are drawn along X and Z axis for $Y = b/2$, and the values of m and n are $1, 2, 3, \ldots, 10$ since here both the odd and the even values of m and n are relevant and none of the $A^{\pm}_{mn}$ coefficients are zero. The results of the analytical and the numerical calculations were compared in Fig. 7 for this case. This figure is in fact the two-dimensional projection of Fig. 6. In Fig. 7 the temperature distribution is drawn along the X axis for $Y = b/2$ at $Z = 0$ and $Z = c/2$ planes. From the figure, it is evident that

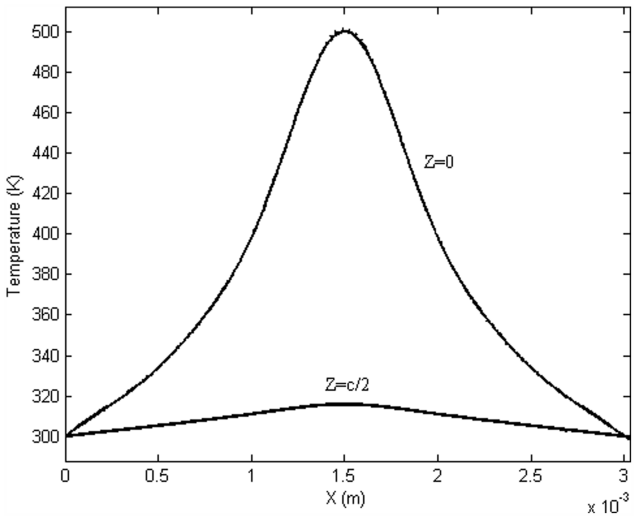

Fig. 3. Temperature distribution at $Z = 0$ and $Z = c/2$ planes along X axis for $P = 15$ W absorbed pump power. Solid curves show our analytical solution with $m, n = 1, 3, 5, 7, 9$; dotted curves show the numerical solution.

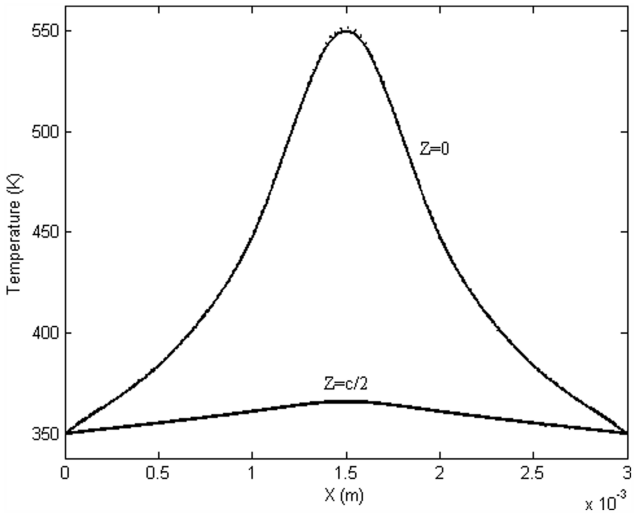

Fig. 5. Temperature distribution along the x direction in the planes $z = 0$ and $z = c/2$ at $y = b/2$, calculated by Eq. (19).

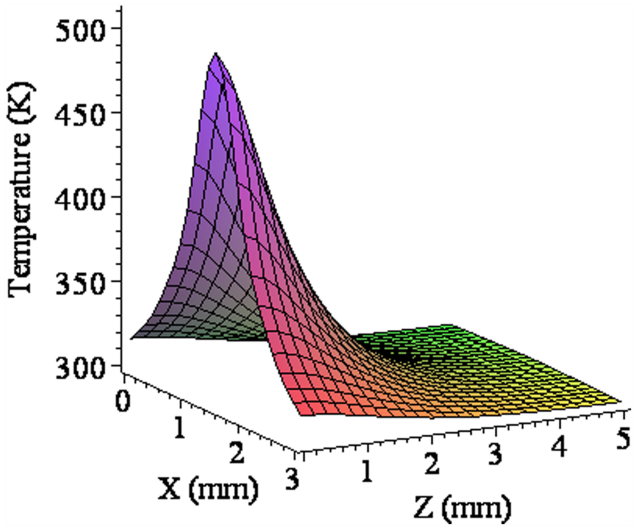

Fig. 6. (Color online) Three-dimensional temperature distribution of Eq. (30) in the X–Z plane at $y = b/2$ with convection cooling boundary conditions for all six faces.

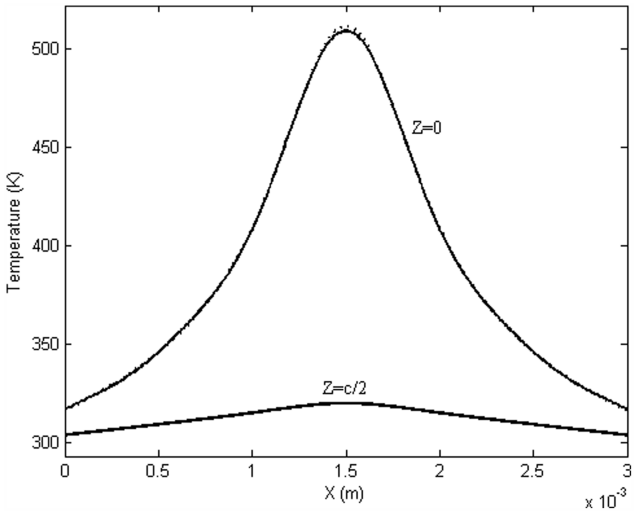

Fig. 7. Comparison between the analytical (solid) and numerical (dotted) temperature along the X direction in the X–Y planes $z = 0$ and $z = c/2$ at $y = b/2$, obtained by Eq. (30).

there is a very tiny and unremarkable difference between the two calculations.

In summary, the analytical and the numerical results for the temperature distribution of an anisotropic cubic crystal show excellent agreement. From this, one can conclude a very high reliability for our analytical calculations allowing it to be utilized well for complex thermal analysis involving crystals with cubic geometry.

5. Conclusions

There are many works in the literature concerning the thermal analysis of laser crystals of simple cylindrical shape. Although there are also few works about slab crystals, to the best of our knowledge there is no comprehensive analytical thermal expression for cubic geometry laser crystals. This paper presents a complete derivation of temperature distribution of an anisotropic cubic crystal. Three different cases for boundary conditions that cover perfect and imperfect cooling mechanisms of the crystal are investigated in detail. The expressions that are reported for the first time were applied to a Nd : YVO_4 cubic crystal, and the results were compared with its numerical counterparts. The comparison shows excellent agreement between the analytical and the numerical solutions; so the analytical expressions can be regarded as a highly reliable formulation and can guide laser designers when complex thermal analysis of laser cavities is encountered .

Appendix A

Here, the expressions for $A_{mn}^{\pm}$ for our three different cases stated in the text are given:

Case I:

$$A_{mn}^{\pm} = B_{mn}\frac{(K_z\Gamma_{mn} \pm h_a)(K_z\gamma - h_a)\,e^{-\gamma c} - (K_z\Gamma_{mn} \mp h_a)(K_z\gamma + h_a)\,e^{\mp\Gamma_{mn}c}}{(K_z\Gamma_{mn} - h_a)^2\,e^{-\Gamma_{mn}c} - (K_z\Gamma_{mn} + h_a)^2\,e^{\Gamma_{mn}c}}. \tag{A1}$$

Case II:

$$A_{mn}^{\pm} = B_{mn}\frac{(K_z\Gamma_{mn} \pm h_a)(K_z\gamma - h_a)\,e^{-\gamma c} - (K_z\Gamma_{mn} \mp h_a)(K_z\gamma + h_a)\,e^{\mp\Gamma_{mn}c}}{(K_z\Gamma_{mn} - h_a)^2\,e^{-\Gamma_{mn}c} - (K_z\Gamma_{mn} + h_a)^2\,e^{\Gamma_{mn}c}} + \frac{16h\,\Delta T}{mn\pi^2}\frac{(K_z\Gamma_{mn} \pm h_a) + (K_z\Gamma_{mn} \mp h_a)\,e^{\mp\Gamma_{mn}c}}{(K_z\Gamma_{mn} - h_a)^2\,e^{-\Gamma_{mn}c} - (K_z\Gamma_{mn} + h_a)^2\,e^{\Gamma_{mn}c}}. \tag{A2}$$

Case III:

$$A_{mn}^{\pm} = B_{mn}\frac{(K_z\Gamma_{mn} \pm h_a)(K_z\gamma - h_a)\,e^{-\gamma c} - (K_z\Gamma_{mn} \mp h_a)(K_z\gamma + h_a)\,e^{\mp\Gamma_{mn}c}}{(K_z\Gamma_{mn} - h_a)^2\,e^{-\Gamma_{mn}c} - (K_z\Gamma_{mn} + h_a)^2\,e^{\Gamma_{mn}c}}. \tag{A3}$$

Appendix B

By substituting Eq. (30) into Eq. (1), we get

$$\sum_{m,n=1}^{\infty}\left[\frac{\mathrm{d}^2T_{mn}(z)}{\mathrm{d}z^2}-\Gamma_{mn}^2T_{mn}(z)\right]\sin\left(\frac{\alpha_m x}{a}+\beta_m\right)\times\sin\left(\frac{\delta_n y}{b}+\theta_n\right)=-S(x,y,z), \tag{B1}$$

where

$$\Gamma_{mn}^2=\frac{K_x}{K_z}\left(\frac{\alpha_m}{a}\right)^2+\frac{K_y}{K_z}\left(\frac{\delta_n}{b}\right)^2 \tag{B2}$$

was defined above in the text. Multiplying both sides by $\sin[(\alpha_{m'}x/a)+\beta_{m'}]\sin[(\delta_{n'}y/b)+\theta_{n'}]$ and integrating over x and y from $0\to a$ and $0\to b$, respectively, we get to

$$\sum_{m,n=1}^{\infty}\left[\frac{\mathrm{d}^2T_{mn}(z)}{\mathrm{d}z^2}-\Gamma_{mn}^2T_{mn}(z)\right]\left[\int_0^a\sin\left(\frac{\alpha_m x}{a}+\beta_m\right)\times\sin\left(\frac{\alpha_{m'}x}{a}+\beta_{m'}\right)\mathrm{d}x\right]\left[\int_0^a\sin\left(\frac{\delta_n y}{b}+\theta_n\right)\times\sin\left(\frac{\delta_{n'}y}{b}+\theta_{n'}\right)\mathrm{d}y\right]=-\frac{16\beta}{K_z ab}s_m t_n e^{-\gamma z}. \tag{B3}$$

To see how these sine functions are orthogonal, we carry out one integral, for example. The second bracket becomes

$$\int_0^a\sin\left(\frac{\alpha_m x}{a}+\beta_m\right)\sin\left(\frac{\alpha_{m'}x}{a}+\beta_{m'}\right)\mathrm{d}x=\frac{a}{2}-\frac{a}{4\alpha}[\sin(2\alpha_m+2\beta_m)-\sin(2\beta_m)] \tag{B4}$$

if $m=m'$ and

$$\int_0^a\sin\left(\frac{\alpha_m x}{a}+\beta_m\right)\sin\left(\frac{\alpha_{m'}x}{a}+\beta_{m'}\right)\mathrm{d}x=\frac{a}{2(\alpha_m-\alpha_{m'})}\times\left\{\sin[(\alpha_m+\beta_m)-(\alpha_{m'}+\beta_{m'})]-\sin(\beta_m+\beta_{m'})\right\}$$
$$=\frac{a}{2(\alpha_m-\alpha_{m'})}[\sin(\alpha_m+\beta_m)\cos(\alpha_{m'}+\beta_{m'})-\cos(\alpha_m+\beta_m)\sin(\alpha_{m'}+\beta_{m'})-\sin(\beta_m)\cos(\beta_m)-\cos(\beta_m)\sin(\beta_m)] \tag{B5}$$

if $m\neq m'$.

Rewriting Eqs. (31) and (32) in the form

$$\sin(\beta_m)=\frac{K_x\alpha_m}{h_s a}\cos(\beta_m), \tag{B6}$$

$$\sin(\alpha_m+\beta_m)=-\frac{K_x\alpha_m}{h_s a}\cos(\alpha_m+\beta_m) \tag{B7}$$

and substituting into (B5), we end up with zero for (B5); i.e., the sinusoidal functions appearing in Eq. (30) are orthogonal under the convection boundary conditions of Eqs. (26)–(29).

References

1. W. A. Clarkson, "Thermal effects and their mitigation in end-pumped solid-state laser," J. Phys. D **34**, 2381–2395 (2001).
2. D. C. Brown, "Heat, fluorescence, and stimulated-emission power densities and fractions in Nd:YAG," IEEE J. Quantum Electron. **34**, 560–572 (1998).
3. S. Guy, C. L. Bonner, D. P. Shepherd, D. C. Hanna, A. C. Tropper, and B. Ferrand, "High-inversion densities in Nd:YAG: upconversion and bleaching," IEEE J. Quantum Electron. **34**, 900–909 (1998).
4. C. Pfistner, R. Weber, H. P. Weber, S. Merazzi, and R. Gruber, "Thermal beam distortion in end-pumped Nd:YAG, Nd:GSGG, and Nd:YLF Rods," IEEE J. Quantum Electron. **30**, 1605–1615 (1994).
5. H. Nadgaran and M. Sabaian, "Pulsed pump: thermal effects in solid state lasers under super-Gaussian pulses," Pramana J. Phys. **67**, 1119–1128 (2006).
6. H. Nadgaran and P. Elahi, "The overall phase shift and lens effect calculation using Gaussian boundary conditions and paraxial ray approximation for an end-pumped solid state laser," Pramana J. Phys. **66**, 513–519 (2006).
7. M. Sabaeian and H. Nadgaran, "Bessel–Gauss beams: investigations of thermal effects on their generation," Opt. Commun. **281**, 672–678 (2008).
8. A. K. Cousins, "Temperature and thermal stress scaling in finite-length end-pumped laser rods," IEEE J. Quantum Electron. **28**, 1057–1069 (1992).
9. M. Schmid, Th. Graf, and H. P. Weber, "Analytical model of the temperature distribution and the thermally induced birefringence in laser rods with cylindrically symmetric heating," J. Opt. Soc. Am. B **17**, 1398–1404 (2000).
10. B. A. Usievich, V. A. Sychugov, F. Pigeon, and A. Tishchenko, "Analytical treatment of the thermal problem in axially pumped solid-state lasers," IEEE J. Quantum Electron. **37**, 1210–1214 (2001).
11. H. Zhang, J. Liu, J. Wang, Ch. Wang, L. Zhu, Z. Shao, X. Meng, X. Hu, and M. Jiang, "Characterization of the laser crystal Nd : $GdVO_4$," J. Opt. Soc. Am. B **19**, 18–27 (2002).
12. P. K. Mukhopadhyay, J. George, K. Ranganathan, S. K. Sharma, and T. P. S. Nathan, "An alternative approach to determine the fractional heat load in solid state laser material: application to diode-pumped Nd : YVO_4 laser," Opt. Laser Technol. **34**, 253–258 (2002).
13. R. A. Fields, M. Birnbaun, and C. N. Fincher, "High efficiency Nd : YVO_4 diode-laser end-pumped laser," Appl. Phys. Lett. **51**, 1885–1886 (1987).
14. Z. Ma, D. Li, J. Gao, N. Wu, and K. Du, "Thermal effects of the diode end-pumped Nd : YVO_4 slab," Opt. Commun. **275**, 179–185 (2007).
15. P. Shi, W. Chen, L. Li, and A. Gan, "Semianalytical thermal analysis on a Nd : YVO_4 crystal," Appl. Opt. **46**, 4046–4051 (2007).
16. P. Zeller and P. Peuser, "Efficient, multiwatt, continuous-wave laser operation on the 4F3/2-4I9/2 transitions of Nd : YVO_4 and Nd:YAG," Opt. Lett. **25**, 34–36 (2000).

17. M. J. Damzen, M. Trew, E. Rosas, and G. J. Crofts, "Continuous-wave Nd : YVO_4 grazing-incidence laser with 22.5 W output power and 64% conversion efficiency," Opt. Commun. **196**, 237–241 (2001).
18. Y. F. Chen and S. W. Tsai, "Diode-pumped *Q*-switched Nd : YVO_4 yellow laser with intracavity sum-frequency mixing," Opt. Lett. **27**, 397–399 (2002).
19. Z. Xiong, Z. G. Li, N. Moore, W. L. Huang, and G. C. Lim, "Detailed investigation of thermal effects in longitudinally diode-pumped Nd : YVO_4 lasers," IEEE J. Quantum Electron. **39**, 979–986 (2003).
20. G. Arfken, *Mathematical Methods for Physicists* (Academic, 1988).
21. X. Peng, A. Asundi, Y. Chen, and Zh. Xiong, "Study of the mechanical properties of Nd : YVO_4 crystal by use of laser interferometry and finite-element analysis," Appl. Opt. **40**, 1396–1403 (2001).